

A spinless crystal for a high-performance solid-state ^{229}Th nuclear clock

Harry W. T. Morgan,^{1,2} James E. S. Terhune,³ Ricky Elwell,³ Hoang Bao Tran Tan,^{4,5} Udeshika C. Perera,⁴ Andrei Derevianko,⁴ Eric R. Hudson,^{3,6,7} and Anastassia N. Alexandrova¹

¹*Department of Chemistry and Biochemistry, University of California, Los Angeles, Los Angeles, CA 90095, USA*

²*Department of Chemistry, University of Manchester, Oxford Road, Manchester M13 9PL, UK*

³*Department of Physics and Astronomy, University of California, Los Angeles, CA 90095, USA*

⁴*Department of Physics, University of Nevada, Reno, Nevada 89557, USA*

⁵*Los Alamos National Laboratory, P.O. Box 1663, Los Alamos, New Mexico 87545, USA*

⁶*Challenge Institute for Quantum Computation, University of California Los Angeles, Los Angeles, CA, USA*

⁷*Center for Quantum Science and Engineering, University of California Los Angeles, Los Angeles, CA, USA*

(Dated: March 17, 2025)

Solid-state ^{229}Th nuclear clocks require a host material whose band gap is larger than the 8.4 eV nuclear transition energy. As such, excitation of the ^{229}Th nuclear state has so far only been demonstrated in metal fluorides, specifically CaF_2 , LiSrAlF_6 , and ThF_4 , where the large electronegativity of the halogen leads to sufficient band gaps. However, it is expected that the nuclear magnetic moment of the fluorine gives rise to a leading order broadening mechanism that limits the clock stability. Here, we use concepts of molecular design to identify a polyatomic anion, SO_4^{2-} , that is both nuclear spin free and of sufficient electron affinity to result in a high band gap metal sulfate system. Using state-of-the-art calculations, we find that the band gap of $\text{Th}(\text{SO}_4)_2$ is approximately 9 eV, large enough for direct laser excitation of ^{229}Th . Low concentrations of ^{229}Th in the otherwise spinless $^{232}\text{Th}(\text{SO}_4)_2$ crystal mitigate ^{229}Th - ^{229}Th interactions. Furthermore, the introduction of ^{229}Th does not modify the material band gap nor introduce electronic states associated with nuclear quenching. By removing one of the primary sources of nuclear line broadening in the crystal, the nuclear magnetic dipole-dipole interaction, a nuclear clock with instability as low as $\sigma = 4.6 \times 10^{-23}/\sqrt{\tau}$, where τ is the averaging time, may be realized. This is roughly six orders of magnitude lower than previously thought possible.

The ^{229}Th nuclear isomeric state provides a laser-accessible nuclear transition that can be driven even when doped into a high-band gap solid [1]. This feature should allow a number of exciting applications: the construction of a robust and portable optical nuclear clock [2]; exploration of nuclear superradiance [3]; tests of fundamental physics [1, 4]; a new probe of the solid-state environment [5–7]; and, perhaps, a new temperature standard. Excitement about this concept has erupted since the recent demonstrations of excitation of the ^{229}Th nucleus with an 8.4 eV laser in CaF_2 , LiSrAlF_6 , and ThF_4 [7–9].

A key parameter for these applications is the linewidth of the nuclear transition. As the natural linewidth of the nuclear transition is $\Gamma_n \sim 2\pi \cdot 100 \mu\text{Hz}$, the primary contributions to the transition linewidth come from interaction of the nucleus with the nucleonic degrees of freedom of the crystal; these were analyzed in Ref. [1]. In ionic solids, a chief broadening mechanism was identified as the magnetic dipole-dipole interaction between the ^{229}Th nucleus and the nuclear magnetic moments of nearby atoms. While this broadening can be reduced by techniques like “magic-angle spinning” [10] and dynamical decoupling [11], it would be advantageous to remove it entirely. Here, we identify a crystalline host for ^{229}Th built from atoms without nuclear magnetic moments.

The host crystal for a ^{229}Th nuclear clock must have a band gap larger than 8.4 eV when doped with ^{229}Th to allow excitation of the nuclear transition. It is also de-

sirable that the introduction of ^{229}Th into the material does not create an electronic state that might quench the nuclear excited state non-radiatively [12–15]. For these reasons, the current paradigm in thorium clock material is a metal fluoride system [6–9, 16–22], as fluorine is the most electronegative element [23]. In these materials, however, the nuclear magnetic dipole-dipole interaction of the ^{229}Th nucleus with the surrounding ^{19}F nuclei leads to an inhomogeneous broadening of order 1–10 kHz [1, 7]. This is expected to be the primary limit of clocks based on these materials, leading to predicted instabilities of $\sigma \sim 10^{-15} - 10^{-17}/\sqrt{\tau}$, where τ is the averaging time.

Options for spinless atomic anion replacements are limited. While other halogens have large electronegativities, they are all spinful. On the other hand, S and O both have predominant zero-spin isotopes, but thorium dioxide and disulfide have small band gaps [24–26]. Inspired by the molecular design principles of “superhalogens” and strong acids, we posit that the sulfate anion, SO_4^{2-} , could provide a molecular solution to this problem [27–30]. This anion has strong S-O bonds and exhibits delocalization of the negative charges, thus electron transfer from SO_4^{2-} to a metal cation like Th^{4+} has a large energy cost. This suggests that $\text{Th}(\text{SO}_4)_2$ could combine the favorable nuclear properties of O and S with the electronic properties needed for a large band gap. Further, as $\text{Th}(\text{SO}_4)_2$ is a stoichiometric material, there is no interference from the charge-compensating defects that form

in the metal fluorides [6, 17, 18, 22, 31].

The synthesis and structural characterization of $\text{Th}(\text{SO}_4)_2$ have been reported in the literature [32–34]. The unit cell, shown in Fig. 1(a), contains eight thorium atoms, all in the same chemical environment. Each thorium atom is coordinated to eight oxygen atoms in approximately square antiprismatic geometry, as shown in Fig. 1(b). The sulfate anion itself has the S atom in the center and the O atoms arranged in a tetrahedron, as shown in Fig. 1(c). The two negative charges are spread equally over the four O atoms and all four S-O bond lengths are equal to within 0.01 Å.

The band gap of $\text{Th}(\text{SO}_4)_2$ appears to be unknown. Therefore, in what follows, we report the first calculation of the $\text{Th}(\text{SO}_4)_2$ band gap, based on high-level GW calculations. These calculations determine that the band gap is approximately 9 eV and sufficient for driving the ^{229}Th nuclear excitation. We also discuss the performance of a nuclear clock based on this material and estimate the optimum ^{229}Th concentration, which is determined by balancing the increased signal-to-noise ratio that comes with more ^{229}Th with the concomitant increase in ^{229}Th - ^{229}Th nuclear spin coupling.

The essential quantity for a stoichiometric thorium clock material is the band gap. Density functional theory (DFT) is used widely in materials modeling, but it is ineffective for accurately computing band gaps. Even hybrid functionals, which attempt to improve the description of electronic interactions by including exchange terms from Hartree-Fock theory, may underestimate the band gaps of wide-gap insulators. More accurate predictions come from the GW approach, an approximate many-body theory much more suitable than DFT for excited state properties [35–39]. GW calculations are far more computationally expensive than DFT, however, scaling quartically with the system size and requiring large numbers of virtual orbitals to be included in the calculation. This typically restricts the use of GW calculations to simple structures with few atoms in the unit cell, and only Γ -point sampling of the Brillouin zone. For an accurate prediction of the band gap of $\text{Th}(\text{SO}_4)_2$, we use G_0W_0R , a variation of the more common “single-shot” G_0W_0 method with reduced computational scaling at the expense of higher memory usage [40, 41]. This calculation yields a band gap of 9.08 eV, which is large enough to allow laser excitation of ^{229}Th at 8.4 eV. Further, as G_0W_0 and G_0W_0R typically *underestimate* band gaps by 5–10% [35–38, 40, 41], $\text{Th}(\text{SO}_4)_2$ appears promising as a host for a nuclear clock with performance significantly beyond the materials considered to date. Details of the computational method and comparisons to other methods can be found in the supplemental information.

These calculations, along with the known structure of $\text{Th}(\text{SO}_4)_2$, also allow a detailed analysis of the nuclear structure and estimation of nuclear clock performance. The ^{229}Th nuclear transition occurs between states $I_e =$

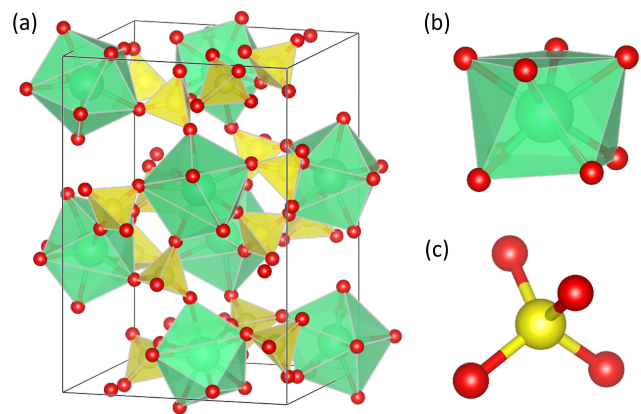


FIG. 1. Crystal structure of thorium sulfate $\text{Th}(\text{SO}_4)_2$. (a) Unit cell. All Th atoms are related by symmetry. (b) ThO_8 coordination shell. (c) SO_4^{2-} anion. Th atoms are shown in green, S in yellow, and O in red.

$3/2^+[631]$ and $I_g = 5/2^+[633]$ – where the numbers in brackets are the standard Nilsson quantum numbers – and therefore exhibits hyperfine structure due to both the electric quadrupole and magnetic dipole moments of the nuclear states, following the Hamiltonian [42]:

$$\hat{H} = -\mu_\alpha \vec{I} \cdot \vec{B} + \frac{eQ_\alpha V_{zz}}{4I(2I-1)} \left[3\hat{I}_z^2 - \hat{I}^2 + \eta(\hat{I}_x^2 - \hat{I}_y^2) \right] \quad (1)$$

where μ_α is the nuclear magnetic dipole moment, Q_α is the nuclear electric quadrupole moment, \hat{I} is the total nuclear spin operator, $\hat{I}_{x,y,z}$ are the components of the nuclear spin operators, $V_{xx,yy,zz}$ are the components of the electric field gradient (EFG) at the nucleus, $\eta = |V_{xx} - V_{yy}|/V_{zz}$ is the EFG asymmetry parameter with the choice $|V_{zz}| > |V_{xx}| > |V_{yy}|$, and $\alpha = \{g, e\}$ denotes the ground and excited nuclear states, respectively. The interaction of the nuclear electric quadrupole moment with the crystal EFG is the largest interaction. The Th atoms in $\text{Th}(\text{SO}_4)_2$ are symmetry equivalent, thus all ^{229}Th experience the same EFG magnitude. Using DFT, we calculate the electric field gradient at the nucleus to be $V_{zz} = 200.4 \text{ V}/\text{\AA}^2$ with $\eta = 0.605$, resulting in the hyperfine level splittings shown in the supplementary information (SI) [43].

In a crystalline host made of spinless atoms, the doped ^{229}Th nuclei couple via the magnetic dipole-dipole and electric quadrupole-quadrupole interactions [1]; ignoring spin-exchange type interactions, the relative strength of these mechanisms can be roughly estimated as $E_{dd} \approx \mu^2 \mu_0 / (2\pi r^3)$ and $E_{QQ} \approx 6Q^2 / (4\pi \epsilon r^5)$, respectively. Using the parameters of the ground state ($\mu \approx 0.36 \mu_N$ and $Q \approx 3.11 \text{ eb}$ [44]), estimating the dielectric constant of $\text{Th}(\text{SO}_4)_2$ as $\epsilon = 10$ based on other metal sulfates [45], and evaluating at the minimum Th-Th distance in the optimized $\text{Th}(\text{SO}_4)_2$ structure, $r = 5.033 \text{ \AA}$, one finds $E_{dd} \sim 10 \text{ Hz}$ and $E_{QQ} \sim 0.001 \text{ Hz}$. Therefore, in what

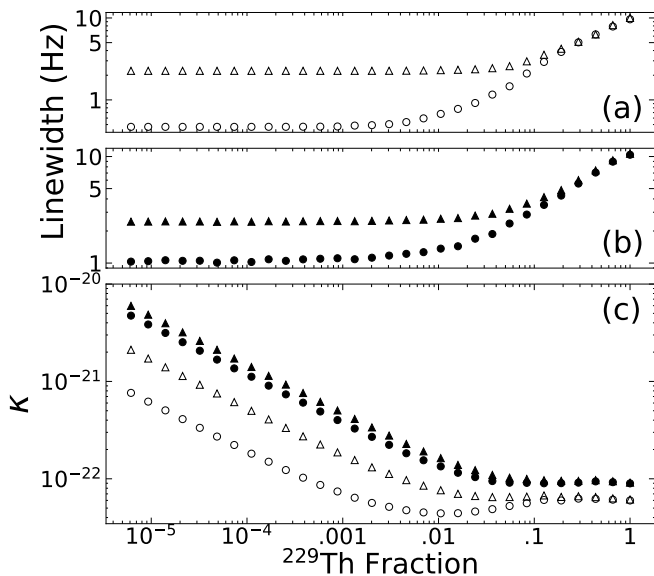


FIG. 2. For isotopically pure (a) and natural abundance (b) S and O, the ^{229}Th transition linewidth due to crystal effects as a function of the ratio of ^{229}Th to ^{232}Th . (c) The minimal instability of a solid-state clock based on $\text{Th}(\text{SO}_4)_2$ is given as $\sigma = \kappa/\sqrt{\tau}$, where τ is the averaging time. In both figures, the unfilled points correspond to isotopically pure ^{16}O and ^{32}S , the filled points correspond to O and S in their natural abundances, the triangles correspond to room temperature operation, and the circles correspond to low temperature operation.

follows, we focus solely on the magnetic dipole-dipole interaction.

Naturally occurring ^{232}Th has no nuclear spin, therefore substituting low concentrations of the spinful clock isotope ^{229}Th increases the distance between the nuclear magnetic dipoles, reducing their interaction. Thus, the broadening depends on the fraction of ^{232}Th that have been substituted with a ^{229}Th atom. To estimate this line broadening as a function of ^{229}Th fraction, we perform a Monte Carlo simulation where each thorium atom in a simulated crystal volume is probabilistically determined to be ^{232}Th or ^{229}Th , with spin-possessing ^{229}Th nuclei treated as classical magnetic dipoles with randomly chosen orientations. The random distribution of ^{229}Th nuclei over the available sites is a good model for a crystal at equilibrium, but may not be accurate for other situations, e.g. if ^{229}Th were introduced by ion beam deposition [15, 46, 47]. The net magnetic field generated by these nuclei is calculated at the position of a ^{229}Th at the center of the simulated crystal volume, and the resulting Zeeman-shifted transition frequency is found according to Eq. (1); this process is repeated to produce a distribution of Zeeman-shifted frequencies and the resulting full width at half maximum (FWHM) of the distribution is used to estimate the inhomogeneously broadened linewidth – see SI for details regarding the simulation and

the crystal volume necessary for convergence. Assuming the $\text{Th}(\text{SO}_4)_2$ host contains only the spinless ^{16}O and ^{32}S , the calculated magnetic dipole broadening increases from < 0.01 Hz to approximately 10 Hz as the ^{229}Th fraction is increased from $\approx 10^{-4}\%$ to 100%. While isotopically pure ^{16}O and ^{32}S are readily available, we also perform the simulation choosing the S and O isotopes according to their natural abundances. This introduces a small fraction of spinful ^{33}S (0.763%, $I = 3/2$) and ^{17}O (0.0367%, $I = 5/2$), which at low ^{229}Th concentration raises the observed linewidth to ≈ 1 Hz.

As these magnetic-dipole-broadened linewidths are roughly three orders of magnitude smaller than that expected in the metal fluorides previously considered, other sources of broadening and shifts must also be considered in $\text{Th}(\text{SO}_4)_2$. The so-called isomer shift contains both the second-order Doppler shift (SODS) and the intrinsic isomer shift, which characterizes the shift in the nuclear transition frequency due to the monopole interaction between the nucleons and the electronic density at the nucleus [5, 48]. Both the isomer and quadrupole shifts are temperature dependent [1], so thermal gradients across the crystal lead to another source of inhomogeneous broadening.

Using the Debye model of solids, along with typical values found in Mößbauer spectroscopy, we estimate the SODS, the intrinsic isomer shift, and electric quadrupole shift to have temperature dependencies of roughly 1 Hz/K [49], 5 kHz/K [48, 50–53], and 25 kHz/K [53–62], respectively, at room temperature (see SI). With a 0.1 mK thermal gradient, the SODS will contribute negligible broadening, while the intrinsic isomer shift and electric quadrupole shift will contribute approximately 0.5 and 2.5 Hz to the linewidth, respectively.

The temperature dependence of both the intrinsic isomer shift and the electric quadrupole shift can be viewed as resulting from a change in the crystal bond lengths with temperature and, as such, lead to shifts that are proportional to $\alpha\Delta T/T$, where α is the coefficient of thermal expansion of the host material. At temperatures well below the Debye temperature, the atoms of a crystal only explore the harmonic portion of their bonding potential and, generically, $\alpha \rightarrow 0$ as $T \rightarrow 0$. As a result, the temperature dependence of these shifts decrease as temperature decreases [54–62]. Using typical values from Mößbauer spectroscopy, we estimate that the SODS will again contribute negligible broadening, while the intrinsic isomer shift and electric quadrupole shift will have broadenings of roughly 0.1 Hz and 0.4 Hz, respectively, at 4 K (see SI).

With these results, the linewidth of the thorium isomeric transition can be estimated and the quadrature sum of these broadening mechanisms is shown in Fig. 2(a)-(b) as a function of ^{229}Th concentration. In both cases, the linewidth rises as the ^{229}Th fraction passes about 0.1% due to increasing magnetic dipole-

dipole interaction between ^{229}Th nuclei. At ^{229}Th fractions below 0.1%, the linewidth is set by the temperature dependent broadenings in the case of spinless S and O atoms or by the interaction with magnetic dipole moments of the ^{33}S and ^{17}O for the case of naturally abundant S and O atoms. It is also assumed that the fraction f of ^{229}Th that undergo recoilless emission or absorption is near unity, where f is the Lamb-Mössbauer factor [63]. Using the Debye model, the ratio of inelastic to elastic scattering of photons is $\sim 10^{-8}$ across a wide range below the Debye temperature. Therefore, any ‘‘Doppler’’ broadening due to coupling to motional sidebands is negligible.

The instability of a nuclear clock based on $\text{Th}(\text{SO}_4)_2$ using fluorescence collection can be estimated as $\sigma = 1/(2\pi QS)\sqrt{(T_e + T_c)/\tau} = \kappa/\sqrt{\tau}$, where $Q = f_0/\Delta f$ is the quality factor, S is the signal-to-noise ratio, T_e is the excitation time, T_c is the collection time, and τ is the averaging time [64]; here we assume S is shot-noise limited with $S = N_d/\sqrt{N_d + T_c b}$, where N_d is the number of fluorescence photons collected and b is the background photon count rate. When calculating N_d , it is assumed that photons can be collected with a 1% efficiency rate. To include the effects of power broadening and a finite laser linewidth, the inhomogeneous Zeeman spectrum is convolved with the excitation spectrum obtained from the optical Bloch equations, assuming a clock laser of power 1 μW with a 1 Hz linewidth. The FWHM of this convolved line shape is then added in quadrature with the inhomogeneous intrinsic isomer and electric quadrupole broadenings to obtain Δf . Next, in the metal fluorides explored to date, the background count rate is dominated by radiation induced phosphorescence. This process depends sensitively on the details of the material and is therefore difficult to predict. Therefore, we estimate from that observed in $^{229}\text{Th}:\text{LiSrAlF}_6$ as $b = 2 \times 10^2 (n_{\text{Th}229}/5 \times 10^{15} \text{ cm}^{-3})$, where $n_{\text{Th}229}$ is the number density of ^{229}Th in $\text{Th}(\text{SO}_4)_2$. Similarly, as the lifetime of the isomeric state in $\text{Th}(\text{SO}_4)_2$ is unknown, we approximate it using the value of 573 s measured in $^{229}\text{Th}:\text{LiSrAlF}_6$ [12]. The resulting κ , which can roughly be viewed as the clock instability at 1 s even though a true clock cycle would presumably be longer, is shown in Fig. 2(c), where the values $T_c = 87$ s and $T_e = 5$ s are used to minimize κ .

The instability is minimized at a ^{229}Th fraction of 1% with $\sigma \approx 5 \times 10^{-23}/\sqrt{\tau}$ for spinless S and O atoms. That ratio corresponds to a density of ^{229}Th at $4.5 \times 10^{19} \text{ cm}^{-3}$. This minimum in σ exists as a compromise between the increase in S and increase in linewidth as ^{229}Th fraction is increased. For naturally abundant S and O atoms, the spinful ^{17}O and ^{33}S isotopes broaden the linewidth by roughly 1 Hz. This results in a minimum stability of $\sigma \approx 9 \times 10^{-23}/\sqrt{\tau}$ at a ^{229}Th fraction of 100%.

Finally, the accuracy of a nuclear clock based on $\text{Th}(\text{SO}_4)_2$ is currently expected to be limited by the

ability to accurately set the average temperature of the crystal. Given that platinum resistive thermometers provide a temperature accuracy of roughly 1 part per million [65, 66], it is expected that the temperature dependence of the intrinsic isomer and electric quadrupole shifts lead to a fractional frequency inaccuracy of roughly 4×10^{-15} at room temperature and roughly 8×10^{-17} at 4 K. Given this inaccuracy is substantially above the instability, these systems, beyond nuclear timekeeping, would appear to be useful also as a new type of thermometer. Further, it is likely that co-thermometry using multiple transitions within the nuclear hyperfine structure, possessing different temperature sensitivity, can be used to lower the inaccuracy.

While the projected inaccuracy is comparable to what is expected for metal fluoride nuclear clocks, the projected instability is 5-6 orders of magnitude lower. This is a consequence of a reduction in transition linewidth by three orders of magnitude and the use of a higher ^{229}Th concentration, made possible by the fact that Th is native to the otherwise spinless $\text{Th}(\text{SO}_4)_2$ lattice. Such a large improvement could open completely new avenues for timekeeping, geodesy, navigation, searching for ultra-light dark matter [67], and multi-messenger astronomy in exotic physics modality [68].

In summary, to achieve the large band gap necessary for driving the 8.4 eV ^{229}Th nuclear transition, currently employed hosts for planned ^{229}Th nuclear clocks are all metal fluorides, e.g. CaF_2 [8], LiSrAlF_6 [6], ThF_4 [7], and BaMgF_4 [22]. However, the nuclear magnetic moment of the fluorine in these crystals leads to broadening of the nuclear clock transition by 1-10 kHz. Unfortunately, atomic spinless anions that have a sufficient electron affinity to achieve the necessary band gap are unavailable, e.g. metal sulfides and metal oxides have low band gaps [24–26]. Therefore, we have used concepts of molecular design to identify the sulfate anion, SO_4^{2-} , that is both spinless and results in a large band gap when bonded with Th. We find from state-of-the-art *GW* electronic structure calculations that thorium sulfate, $\text{Th}(\text{SO}_4)_2$, appears suitable as a crystalline host for a solid-state ^{229}Th nuclear clock, with a band gap of 9.08 eV. Using the determined structure, we estimate the performance of a ^{229}Th -doped $\text{Th}(\text{SO}_4)_2$ nuclear clock as a function of ^{229}Th fraction. We find that when using spinless S and O atoms, a minimum clock instability of $\sigma \approx 5 \times 10^{-23}/\sqrt{\tau}$ is achievable at a ^{229}Th fraction of 1%; when natural abundances of S and O isotopes are used, a similar performance is available near 100% ^{229}Th fraction. In addition to mitigation of magnetic dipole-dipole broadening, since the material is stoichiometric, a high, controllable ^{229}Th density and a uniform chemical environment are straightforward to achieve, without the introduction of electronic defects that can quench the nuclear excitation [14, 15]. As a result, ^{229}Th -doped $\text{Th}(\text{SO}_4)_2$ may offer a nuclear clock of unprecedented per-

formance with wide ranging impacts in timekeeping, navigation, and the search for physics beyond the standard model.

ACKNOWLEDGEMENTS

This work was supported by NSF awards PHYS-2013011, PHY-2207546, PHY-2412869 and ARO award W911NF-11-1-0369. This work used Bridges-2 at Pittsburgh Supercomputing Center through allocation PHY230110 from the ACCESS program, which is supported by NSF grants #2138259, #2138286, #2138307, #2137603, and #2138296.

-
- [1] W. Rellergert, D. DeMille, R. Greco, M. Hehlen, J. Torgerson, and E. Hudson, Constraining the evolution of the fundamental constants with a solid-state optical frequency reference based on the ^{229}Th nucleus, *Physical Review Letters* **104**, 10.1103/PhysRevLett.104.200802 (2010).
- [2] W. Rellergert, S. Sullivan, D. DeMille, R. Greco, M. Hehlen, R. Jackson, J. Torgerson, and E. Hudson, Progress towards fabrication of ^{229}Th -doped high energy band-gap crystals for use as a solid-state optical frequency reference, in *11th Europhysical Conference on Defects in Insulating Materials (EURODIM 2010)*, Vol. 15.
- [3] E. Tkalya, Proposal for a nuclear gamma-ray laser of optical range, *Physical Review Letters* **106**, 10.1103/PhysRevLett.106.162501 (2011).
- [4] E. Peik, T. Schumm, M. Safronova, A. Pálffy, J. Weitenberg, and P. Thirolf, Nuclear clocks for testing fundamental physics, *Quantum Science and Technology* **6**, 10.1088/2058-9565/abe9c2 (2021).
- [5] P. Gütlich, C. Schröder, and V. Schünemann, Mössbauer spectroscopy—an indispensable tool in solid state research, *Spectroscopy Europe/World* **24**, 21 (2012).
- [6] R. Elwell, C. Schneider, J. Jeet, J. Terhune, H. Morgan, A. Alexandrova, H. Tan, A. Derevianko, and E. Hudson, Laser excitation of the ^{229}Th nuclear isomeric transition in a solid-state host, *Physical Review Letters* **133**, 10.1103/PhysRevLett.133.013201 (2024).
- [7] C. K. Zhang, L. von der Wense, J. F. Doyle, J. S. Higgins, T. Ooi, H. U. Friebel, J. Ye, R. Elwell, J. E. S. Terhune, H. W. T. Morgan, A. N. Alexandrova, H. B. T. Tan, A. Derevianko, and E. R. Hudson, $^{229}\text{ThF}_4$ thin films for solid-state nuclear clocks, *Nature* **636**, 10.1038/s41586-024-08256-5 (2024).
- [8] J. Tiedau, M. Okhapikin, K. Zhang, J. Thielking, G. Zitzer, E. Peik, F. Schaden, T. Pronebner, I. Morawetz, L. De Col, F. Schneider, A. Leitner, M. Pressler, G. Kazakov, K. Beeks, T. Sikorsky, and T. Schumm, Laser excitation of the ^{229}Th nucleus, *Physical Review Letters* **132**, 10.1103/PhysRevLett.132.182501 (2024).
- [9] C. Zhang, T. Ooi, J. S. Higgins, J. F. Doyle, L. von der Wense, K. Beeks, A. Leitner, G. A. Kazakov, P. Li, P. G. Thirolf, T. Schumm, and J. Ye, Frequency ratio of the $^{229\text{m}}\text{Th}$ nuclear isomeric transition and the ^{87}Sr atomic clock, *Nature* **633**, 63 (2024).
- [10] P. Anisimov, Y. Rostovtsev, and O. Kocharovskaya, Concept of spinning magnetic field at magic-angle condition for line narrowing in mossbauer spectroscopy, *Physical Review B* **76**, 10.1103/PhysRevB.76.094422 (2007).
- [11] A. Ajoy, R. Nirodi, A. Sarkar, P. Reshetikhin, E. Druga, A. Akkiraju, M. McAllister, G. Maineri, S. Le, A. Lin, A. M. Souza, C. A. Meriles, B. Gilbert, D. Suter, J. A. Reimer, and A. Pines, Dynamical decoupling in interacting systems: applications to signal-enhanced hyperpolarized readout (2020), arXiv:2008.08323 [quant-ph].
- [12] J. E. S. Terhune, R. Elwell, H. B. T. Tan, U. C. Perera, H. W. T. Morgan, A. N. Alexandrova, A. Derevianko, and E. R. Hudson, Photo-induced quenching of the ^{229}Th isomer in a solid-state host (2024), arXiv:2412.08998 [physics.atom-ph].
- [13] F. Schaden, T. Riebner, I. Morawetz, L. T. D. Col, G. A. Kazakov, K. Beeks, T. Sikorsky, T. Schumm, K. Zhang, V. Lal, G. Zitzer, J. Tiedau, M. V. Okhapikin, and E. Peik, Laser-induced quenching of the Th-229 nuclear clock isomer in calcium fluoride (2024), arXiv:2412.12339 [physics.atom-ph].
- [14] H. W. T. Morgan, H. B. T. Tan, R. Elwell, A. N. Alexandrova, E. R. Hudson, and A. Derevianko, Theory of internal conversion of the thorium-229 nuclear isomer in solid-state hosts (2024), arXiv:2411.15641.
- [15] S. V. Pineda, P. Chhetri, S. Bara, Y. Elskens, S. Casci, A. N. Alexandrova, M. Au, M. Athanasakis-Kaklamanakis, M. Bartokos, K. Beeks, C. Bernerd, A. Claessens, K. Chrysalidis, T. E. Cocolios, J. G. Correia, H. De Witte, R. Elwell, R. Ferrer, R. Heinke, E. R. Hudson, F. Ivandikov, Y. Kudryavtsev, U. Köster, S. Kraemer, M. Laatiaoui, R. Lica, C. Merckling, I. Morawetz, H. W. T. Morgan, D. Moritz, L. M. C. Pereira, S. Raeder, S. Rothe, F. Schaden, K. Scharl, T. Schumm, S. Stegemann, J. Terhune, P. G. Thirolf, S. M. Tunhuma, P. Van Den Bergh, P. Van Duppen, A. Vantomme, U. Wahl, and Z. Yue, Radiative decay of the $^{229\text{m}}\text{Th}$ nuclear clock isomer in different host materials, *Physical Review Research* **7**, 10.1103/physrevresearch.7.013052 (2025).
- [16] M. Pimon, J. Gugler, P. Mohn, G. A. Kazakov, N. Mauser, and T. Schumm, Dft calculation of (229)thorium-doped magnesium fluoride for nuclear laser spectroscopy, *Journal of Physics-Condensed Matter* **32**, 10.1088/1361-648X/ab7c90 (2020).
- [17] M. Pimon, P. Mohn, and T. Schumm, Band gap calculations for thorium-doped LiCAF, *Advanced Theory and Simulations* **5**, 10.1002/adts.202200185 (2022).
- [18] B. S. Nickerson, M. Pimon, P. V. Bilous, J. Gugler, K. Beeks, T. Sikorsky, P. Mohn, T. Schumm, and A. Pálffy, Nuclear excitation of the ^{229}Th isomer via defect states in doped crystals, *Physical Review Letters* **125**, 10.1103/PhysRevLett.125.032501 (2020).
- [19] B. S. Nickerson, M. Pimon, P. V. Bilous, J. Gugler, G. A. Kazakov, T. Sikorsky, K. Beeks, A. Grüneis, T. Schumm, and A. Pálffy, Driven electronic bridge processes via defect states in ^{229}Th -doped crystals, *Physical Review A* **103**, 10.1103/PhysRevA.103.053120 (2021).
- [20] Q. Gong, S. Tao, S. Li, G. Deng, C. Zhao, and Y. Hang, Feasibility and potential of a thorium-doped barium-lithium-fluoride single crystal as a candidate for solid-state nuclear optical clock material, *Physical Review A*

- 109**, 10.1103/PhysRevA.109.033109 (2024).
- [21] J. Ellis, X. Wen, and R. Martin, Investigation of thorium salts as candidate materials for direct observation of the ^{229}Th nuclear transition, *Inorganic Chemistry* **53**, 6769 (2014).
- [22] H. W. T. Morgan, R. Elwell, J. E. S. Terhune, H. B. T. Tan, U. C. Perera, A. Derevianko, A. N. Alexandrova, and E. R. Hudson, ^{229}Th -doped nonlinear optical crystals for compact solid-state clocks (2024), arXiv:2410.23364.
- [23] A. L. Allred, Electronegativity values from thermochemical data, *Journal of Inorganic & Nuclear Chemistry* **17**, 215 (1961).
- [24] Y. Guo, C. Wang, W. Qiu, X. Ke, P. Huai, C. Cheng, Z. Zhu, and C. Chen, Structural and electronic phase transitions of ThS_2 from first-principles calculations, *Physical Review B* **94**, 10.1103/physrevb.94.134104 (2016).
- [25] T. R. Griffiths and J. Dixon, Electron irradiation of single crystal thorium dioxide and electron transfer reactions, *Inorganica Chimica Acta* **300–302**, 305–313 (2000).
- [26] F. Pereira, M. Castro, M. Vázquez, L. Debán, and A. Aller, Optical properties of ThO_2 -based nanoparticles, *Journal of Luminescence* **184**, 169–178 (2017).
- [27] A. Srivastava, A. Kumar, and N. Misra, Superhalogens as building blocks of ionic liquids, *Journal of Physical Chemistry A* **125**, 2146 (2021).
- [28] A. Srivastava, Recent progress on the design and applications of superhalogens, *Chemical Communications* **59**, 5943 (2023).
- [29] G. Gutsev and A. Boldyrev, Dvm- x_α calculations on the ionization potentials of MX_{k+1} complex anions and the electron affinities of MX_{k+1} super halogens, *Chemical physics* **56**, 277 (1981).
- [30] S. Nielsen and A. Ejsing, On the negative vertical detachment energies of SO_4^{2-} , SeO_4^{2-} , and $\text{SO}_4^{2-}(\text{H}_2\text{O})$, *Chemical Physics Letters* **441**, 213 (2007).
- [31] P. Dessovic, P. Mohn, R. Jackson, G. Winkler, M. Schreitl, G. Kazakov, and T. Schumm, ^{229}Th -doped calcium fluoride for nuclear laser spectroscopy, *Journal of Physics - Condensed Matter* **26**, 10.1088/0953-8984/26/10/105402 (2014).
- [32] U. Betke and M. S. Wickleder, Oleum and sulfuric acid as reaction media: The actinide examples $\text{UO}_2(\text{S}_2\text{O}_7)\text{-lt}$ (low temperature), $\text{UO}_2(\text{S}_2\text{O}_7)\text{-ht}$ (high temperature), $\text{UO}_2(\text{HSO}_4)_2$, $\text{An}(\text{SO}_4)_2$ ($\text{An} = \text{Th}, \text{U}$), $\text{Th}_4(\text{HSO}_4)_2(\text{SO}_4)_7$ and $\text{Th}(\text{HSO}_4)_2(\text{SO}_4)$, *European Journal of Inorganic Chemistry* **2012**, 306–317 (2011).
- [33] A. Abrao, A. de Freitas, and F. de Carvalho, Preparation of highly pure thorium nitrate via thorium sulfate and thorium peroxide, *Journal of alloys and compounds* **323**, 53 (2001).
- [34] A. Albrecht, G. Sigmon, L. Moore-Shay, R. Wei, C. Dawes, J. Szymanowski, and P. Burns, The crystal chemistry of four thorium sulfates, *Journal of Solid State Chemistry* **184**, 1591 (2011).
- [35] M. Shishkin and G. Kresse, Implementation and performance of the frequency-dependent GW method within the paw framework, *Physical Review B* **74**, 10.1103/PhysRevB.74.035101 (2006).
- [36] M. Shishkin and G. Kresse, Self-consistent GW calculations for semiconductors and insulators, *Physical Review B* **75**, 10.1103/PhysRevB.75.235102 (2007).
- [37] W. Chen and A. Pasquarello, Band-edge levels in semiconductors and insulators: Hybrid density functional theory versus many-body perturbation theory, *Physical Review B* **86**, 10.1103/PhysRevB.86.035134 (2012).
- [38] F. Tran and P. Blaha, Accurate band gaps of semiconductors and insulators with a semilocal exchange-correlation potential, *Physical Review Letters* **102**, 10.1103/PhysRevLett.102.226401 (2009).
- [39] M. van Setten, F. Weigend, and F. Evers, The gw-method for quantum chemistry applications: Theory and implementation, *Journal of Chemical Theory and Computation* **9**, 232 (2013).
- [40] P. Liu, M. Kaltak, J. Klimes, and G. Kresse, Cubic scaling GW : Towards fast quasiparticle calculations, *Physical Review B* **94**, 10.1103/PhysRevB.94.165109 (2016).
- [41] H. Rojas, R. Godby, and R. Needs, Space-time method for ab-initio calculations of self-energies and dielectric response functions of solids, *Physical Review Letters* **74**, 1827 (1995).
- [42] S. Thomas, R. Thomas, A. K. Zachariah, and R. K. Mishra, eds., *Spectroscopic Methods for Nanomaterials Characterization*, Micro and Nano Technologies (Elsevier, 2017).
- [43] H. Petrilli, P. Blochl, P. Blaha, and K. Schwarz, Electric-field-gradient calculations using the projector augmented wave method, *Physical Review B* **57**, 14690 (1998).
- [44] M. Safronova, U. Safronova, A. Radnaev, C. Campbell, and A. Kuzmich, Magnetic dipole and electric quadrupole moments of the 229th nucleus, *Physical Review A* **88**, 10.1103/PhysRevA.88.060501 (2013).
- [45] K. F. Young and H. P. R. Frederikse, Compilation of the static dielectric constant of inorganic solids, *Journal of Physical and Chemical Reference Data* **2**, 313–410 (1973).
- [46] M. Verlinde, S. Kraemer, J. Moens, K. Chrysalidis, J. G. Correia, S. Cottenier, H. De Witte, D. V. Fedorov, V. N. Fedosseev, R. Ferrer, L. M. Fraile, S. Geldhof, C. A. Granados, M. Laatiaoui, T. A. L. Lima, P.-C. Lin, V. Manea, B. A. Marsh, I. Moore, L. M. C. Pereira, S. Raeder, P. Van den Bergh, P. Van Duppen, A. Vantomme, E. Verstraelen, U. Wahl, and S. G. Wilkins, Alternative approach to populate and study the ^{229}Th nuclear clock isomer, *Physical Review C* **100**, 10.1103/physrevc.100.024315 (2019).
- [47] S. Kraemer, J. Moens, M. Athanasakis-Kaklamanakis, S. Bara, K. Beeks, P. Chhetri, K. Chrysalidis, A. Claessens, T. E. Cocolios, J. G. M. Correia, H. D. Witte, R. Ferrer, S. Geldhof, R. Heinke, N. Hosseini, M. Huyse, U. Köster, Y. Kudryavtsev, M. Laatiaoui, R. Lica, G. Magchiels, V. Manea, C. Merckling, L. M. C. Pereira, S. Raeder, T. Schumm, S. Sels, P. G. Thirolf, S. M. Tunhuma, P. Van Den Bergh, P. Van Duppen, A. Vantomme, M. Verlinde, R. Villarreal, and U. Wahl, Observation of the radiative decay of the 229th nuclear clock isomer, *Nature* **617**, 706–710 (2023).
- [48] Y. Hazony, $3d$ density distribution and the intrinsic temperature dependence of the mössbauer isomer shift in iron compounds, *Phys. Rev. B* **7**, 3309 (1973).
- [49] K. Tanaka, K. Hirao, and N. Soga, Second-order doppler shift in mössbauer spectra of Fe-B and Fe-P amorphous alloys, *Journal of Applied Physics* **64**, 3299 (1988), <https://pubs.aip.org/aip/jap/article-pdf/64/6/3299/18619632/3299.1.online.pdf>.
- [50] G. M. Rothberg, S. Guimard, and N. Benczer-Koller, Temperature dependence of the β -tin isomer shift, *Phys. Rev. B* **1**, 136 (1970).

- [51] S. T. Lin, G. M. Rothberg, and E. F. Skelton, Temperature dependence of isomer shift of ^{119}Sn in Mg_2Sn and $\beta\text{-Sn}$, *Phys. Rev. B* **10**, 3789 (1974).
- [52] H. K. Perkins and Y. Hazony, Temperature-dependent crystal field and charge density: Mössbauer studies of FeF_2 , KFeF_3 , FeCl_2 , and FeF_3 , *Phys. Rev. B* **5**, 7 (1972).
- [53] J. S. Higgins, T. Ooi, J. F. Doyle, C. Zhang, J. Ye, K. Beeks, T. Sikorsky, and T. Schumm, Temperature sensitivity of a thorium-229 solid-state nuclear clock (2025), arXiv:2409.11590 [physics.atom-ph].
- [54] S. L. Bud'ko, T. Kong, X. Ma, and P. C. Canfield, Study of ^{57}Fe Mössbauer effect in $\text{RFe}_2\text{Zn}_{20}$ ($r = \text{Lu, Yb, Gd}$), *Journal of Physics: Condensed Matter* **27**, 336003 (2015).
- [55] S. I. Shylin, V. Ksenofontov, S. J. Sedlmaier, S. J. Clarke, S. J. Cassidy, G. Wortmann, S. A. Medvedev, and C. Felser, Intercalation effect on hyperfine parameters of Fe in FeSe superconductor with $t_c = 42$ K, *EPL (Europhysics Letters)* **109**, 67004 (2015).
- [56] S. L. Bud'ko, X. Ma, M. Tomić, S. Ran, R. Valentí, and P. C. Canfield, Transition to collapsed tetragonal phase in cafe_2as_2 single crystals as seen by ^{57}Fe mössbauer spectroscopy, *Phys. Rev. B* **93**, 024516 (2016).
- [57] P. Wang, Z. M. Stadnik, J. Żukrowski, A. Thaler, S. L. Bud'ko, and P. C. Canfield, Coexistence of antiferromagnetic ordering and superconductivity in the $\text{ba}(\text{fe}_{0.961}\text{rh}_{0.039})_2\text{as}_2$ compound studied by mössbauer spectroscopy, *Phys. Rev. B* **84**, 024509 (2011).
- [58] A. Gerard and F. Grandjean, Mössbauer spectra in the presence of a fluctuating electric field gradient—applications to the cases of semi-metallic compounds, *Journal of Physics and Chemistry of Solids* **36**, 1365 (1975).
- [59] M. A. Albedah, F. Nejdassattari, Z. M. Stadnik, Y. Liu, and G.-H. Cao, Mössbauer spectroscopy measurements on the 35.5 K superconductor $\text{Rb}_{1-\delta}\text{EuFe}_4\text{As}_4$, *Phys. Rev. B* **97**, 144426 (2018).
- [60] M. A. Albedah, F. Nejdassattari, Z. M. Stadnik, Z.-C. Wang, C. Wang, and G.-H. Cao, Absence of the stripe antiferromagnetic order in the new 30 K superconductor ThFeAsN , *Journal of Alloys and Compounds* **695**, 1128 (2017).
- [61] P. Wang, Z. M. Stadnik, J. Żukrowski, A. Thaler, S. L. Bud'ko, and P. C. Canfield, Coexistence of antiferromagnetic ordering and superconductivity in the $\text{Ba}(\text{Fe}_{0.961}\text{Rh}_{0.039})_2\text{As}_2$ compound studied by mössbauer spectroscopy, *Phys. Rev. B* **84**, 024509 (2011).
- [62] K. Al-Qadi, P. Wang, Z. M. Stadnik, and J. Przewoźnik, Structural, magnetic, and mössbauer spectral study of the icosahedral quasicrystal $\text{Zn}_{77}\text{Fe}_7\text{Sc}_{16}$, *Phys. Rev. B* **79**, 224202 (2009).
- [63] A. Razdan, Lamb–mössbauer factor using non-extensive statistics, *Physics Letters A* **321**, 190 (2004).
- [64] M. M. Boyd, *High Precision Spectroscopy of Strontium in an Optical Lattice: Towards a New Standard for Frequency and Time*, Ph.D. thesis, University of Colorado, Boulder (2007).
- [65] J. V. Widiatmo, I. Saito, and T. Nakano, Evaluation of high-temperature platinum resistance thermometers based on ITS-90, *International Journal of Thermophysics* **41**, 10.1007/s10765-020-2617-y (2020).
- [66] T. Nakano, Stability of standard platinum resistance thermometers and rhodium iron resistance thermometers for the past decade in nmij/aist, *International Journal of Thermophysics* **38**, 10.1007/s10765-017-2201-2 (2017).
- [67] E. Fuchs, F. Kirk, E. Madge, C. Paranjape, E. Peik, G. Perez, W. Ratzinger, and J. Tiedau, Implications of the laser excitation of the Th-229 nucleus for dark matter searches (2024), arXiv:2407.15924 [hep-ph].
- [68] C. Dailey, C. Bradley, D. F. Jackson Kimball, I. A. Sulai, S. Pustelny, A. Wickenbrock, and A. Derevianko, Quantum sensor networks as exotic field telescopes for multimessenger astronomy, *Nature Astronomy* **5**, 150 (2021), arXiv:2002.04352.
- [69] G. Kresse and J. Furthmüller, Efficient iterative schemes for ab initio total-energy calculations using a plane-wave basis set, *Physical Review B* **54**, 11169 (1996).
- [70] P. E. Blochl, Projector augmented wave method, *Physical Review B* **50**, 17953 (1994).
- [71] J. P. Perdew, K. Burke, and M. Ernzerhof, Generalized gradient approximation made simple, *Physical Review Letters* **77**, 3865 (1996).
- [72] V. Wang, N. Xu, J. Liu, G. Tang, and W. Geng, Vaspkit: A user-friendly interface facilitating high-throughput computing and analysis using vasp code, *Computer physics communications* **267**, 10.1016/j.cpc.2021.108033 (2021).

SUPPLEMENTAL INFORMATION

COMPUTATIONAL METHODS FOR ELECTRONIC STRUCTURE THEORY

Calculations were performed with VASP [69], version 6.4.2, using the PAW [70] method. The crystal structure of $\text{Th}(\text{SO}_4)_2$ was optimized using PBE [71] functional, with a k -point spacing of 0.03 \AA^{-1} (4-3-2 Monkhorst-Pack mesh) and a 500 eV plane wave cutoff. The optimized structure was used for subsequent electronic structure calculations. k -point grids were generated with VASPKIT [72].

The band gap of $\text{Th}(\text{SO}_4)_2$ was computed with the G_0W_0R method as implemented in VASP [35, 36, 40, 41]. The method is similar to the non-self-consistent G_0W_0 in which orbitals are computed with DFT and then energy corrections are computed in a single iteration of GW . G_0W_0R differs from G_0W_0 in that the latter scales as N^4 while the former scales as N^3 but has higher memory requirements. G_0W_0R is therefore suitable for larger systems. We tested the agreement between the two by applying both to ThO_2 , getting band gaps of 6.36 eV with G_0W_0 and 6.07 with G_0W_0R .

When calculating the band gap of $\text{Th}(\text{SO}_4)_2$ with G_0W_0R we tested parameters in the method to ensure that the results were not sensitive to them. These parameters include the number of frequency and time grid points used in the calculation (NOMEGA), the DFT method used to generate the orbitals, and the pseudopotentials for sulfur and oxygen. A specialized GW pseudopotential for thorium is not available. The results of these tests are shown in Table I. The important conclusions are that the band gap is converged when NOMEGA = 16, the gap is not sensitive to the choice of DFT orbitals, and the GW pseudopotentials do not make a significant difference to the gap for this system. In the main text we report the band gap of 9.08 eV that was computed with NOMEGA = 16, GW pseudopotentials for O and S, and PBE orbitals. For all calculations on $\text{Th}(\text{SO}_4)_2$ the plane wave cut-off was 400 eV and the k -point spacing was 0.05 \AA^{-1} (2-2-1 Γ -centered mesh).

INHOMOGENOUS ZEEMAN BROADENING SIMULATION

In $\text{Th}(\text{SO}_4)_2$, the only nuclei that will generate a magnetic field are ^{229}Th , ^{17}O , and ^{33}S . For this calculation, these nuclei are treated as classical magnetic dipoles with a random orientation. The assumption of random orientation is only valid at sufficiently high temperature; at low enough temperatures, the populations of different m_I sub-levels will be Boltzmann distributed and the orientation of spin-possessing nuclei would be dictated by the orientation of the crystal's EFG. The positions of

	NOMEGA	Band gap (eV)
PBE orbitals, normal PPs	10	8.84
	12	8.97
	16	8.96
PBE orbitals, GW PPs	12	9.09
	16	9.08
LDA orbitals, GW PPs	12	9.17

TABLE I. Band gap of $\text{Th}(\text{SO}_4)_2$ computed with G_0W_0R with different parameters. ‘‘PP’’ stands for ‘‘pseudopotential’’ and denotes whether the standard or GW -specialized pseudopotentials were used for oxygen and sulfur.

the nuclei are set according to the optimized $\text{Th}(\text{SO}_4)_2$ structure used in the analysis of $\text{Th}(\text{SO}_4)_2$'s electronic properties for consistency.

To calculate the linewidth broadening caused by the nuclei, a simulation is performed as follows. The magnetic field generated by lattice nuclei is calculated at the center of the supercell where a ^{229}Th atom is located. The Zeeman shift due to this net magnetic field is calculated. This ‘‘simulation trial’’ is repeated many times with many different sets of randomized orientations in order to simulate the various magnetic field environments that ^{229}Th may experience. In each simulation trial, only a subset of nuclei are chosen to generate a magnetic field; the ^{17}O and ^{33}S are chosen according to their natural abundances and the ^{229}Th are chosen according to the ^{229}Th fraction. In addition, the chosen lattice nuclei are within a spherical region, centered on a ^{229}Th nucleus, that is large enough that the linewidth does not increase upon further expansion of the sphere. To find a sufficiently large radius, the linewidth was calculated for various radii; it was found that the linewidth converges to a constant value with a radius of $r = 32\text{\AA}$. A spherical region of this size contains 894 Th.

After 75,000 simulation trials, a smooth distribution of Zeeman shifts can be calculated. This distribution corresponds to the inhomogeneously broadened line of only 1 transition. Generally, for a given laser polarization and frequency, and in the absence of static magnetic fields, there will be 4 transitions that are simultaneously driven. This work only considers the $|I = 5/2, m_I = \pm 1/2\rangle \leftrightarrow |3/2, \pm 1/2\rangle$ set of transitions as this is the narrowest spectral line. The observed spectral line is the weighted sum of these 4 transition lines where each transition is weighted according to its Clebsch-Gordan coefficient.

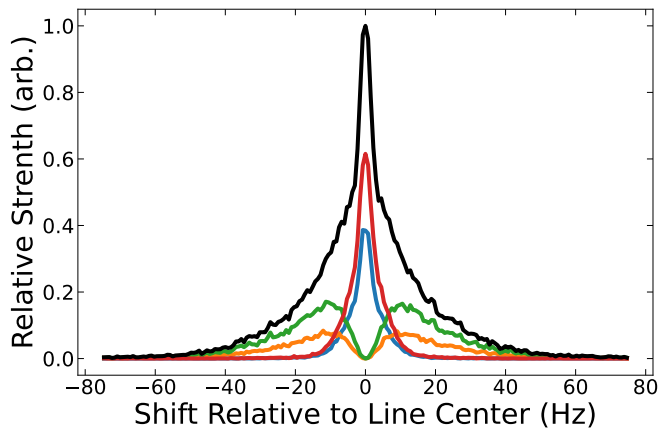


FIG. 3. An inhomogeneously Zeeman broadened spectral line and its components. The laser is linearly polarized with respect to the z-axis defined by the crystal EFG, and the ^{229}Th to ^{232}Th ratio is 0.5. O and S are present in their natural abundances. With the notation $|I = 5/2, m_{I,init}\rangle \leftrightarrow |I = 3/2, m_{I,final}\rangle$, the blue line is $|1/2\rangle \leftrightarrow |-1/2\rangle$, the orange line is $|-1/2\rangle \leftrightarrow |-1/2\rangle$, the green line is $|1/2\rangle \leftrightarrow |1/2\rangle$, the red line is $|-1/2\rangle \leftrightarrow |1/2\rangle$, and the black line is the weighted sum of all transitions.

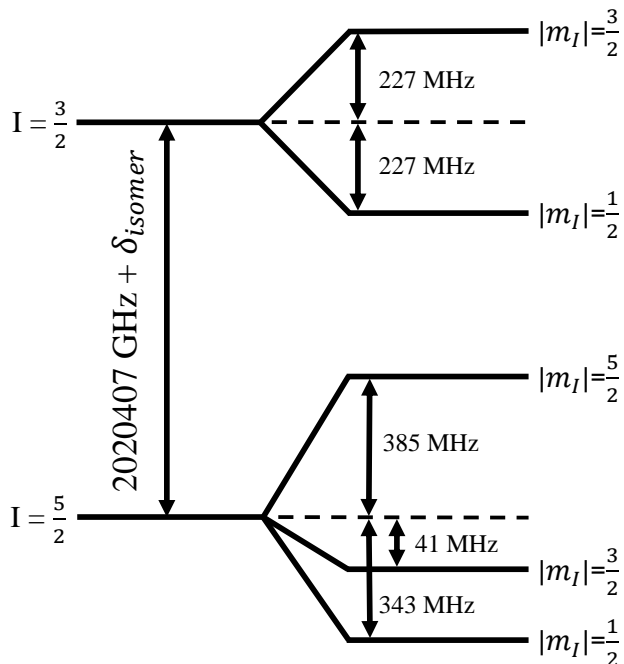


FIG. 4. Hyperfine level splittings of the ground and excited states of ^{229}Th as a result of the electric field gradient of $\text{Th}(\text{SO}_4)_2$.

TEMPERATURE DEPENDENT SHIFTS

Intrinsic Isomer Shift

The isomer shift has 2 distinct contributions: $\delta_{I_s} = \delta_{intrinsic}(T) + \delta_{SOD}(T)$, where $\delta_{intrinsic}$ is the intrinsic isomer shift and δ_{SOD} is the 2nd order Doppler shift (SODS). The intrinsic Doppler shift is a result of the changing electron density at the nucleus due to the temperature-dependent lattice volume. From the Mößbauer literature, typical intrinsic isomer shifts have a temperature dependence of roughly 0.1 - 5 kHz/K [48, 50–53]. Assuming a 0.1 mK temperature gradient, a 5 kHz/K shift will result in a broadening of 0.5 Hz.

2nd Order Doppler Shift

Atoms in a solid will have a non-zero average squared velocity. This gives rise to a SODS, given by: $\delta_{SOD} = -\langle v^2 \rangle / c^2$. In the Debye model of solids, this translates to a shift in the line center given by [49]:

$$\delta_{SOD}(T) = -E_\gamma \frac{3k_B T}{2Mc^2} \times \left(\frac{3\Theta_D}{8T} + 3(T/\Theta_D)^3 \int_0^{\Theta_D/T} \frac{x^3}{e^x - 1} dx \right), \quad (2)$$

where E_γ is the energy of the absorbed/emitted photon and Θ_D is the Debye temperature. Fig. 5a shows the SODS for ^{229}Th as a function of temperature at various common values of the Debye temperature. Fig. 5b shows the 1st temperature derivative of the SODS. As can be seen in Fig. 5b, the SODS no longer varies with temperature at sufficiently low temperatures; for a Debye temperature of 500 K, a crystal temperature of 50 K or lower would eliminate temperature dependence of the SODS. For purposes of clock operation, this would remove a potential source of frequency uncertainty that would originate from temperature sensing inaccuracy. In addition, this would eliminate linewidth broadening that would have been caused by a thermal gradient across the crystal.

As a side note, for this particular nuclear transition, the magnitude of the SODS is significantly reduced compared to other isomeric transitions because the transition energy is comparatively small. Likewise, the intrinsic isomer shift will be the dominant contributor to the total isomer shift. This makes ^{229}Th a good candidate for accurate measurement of intrinsic isomer shifts, which is often difficult since the SODS is usually the dominant contribution.

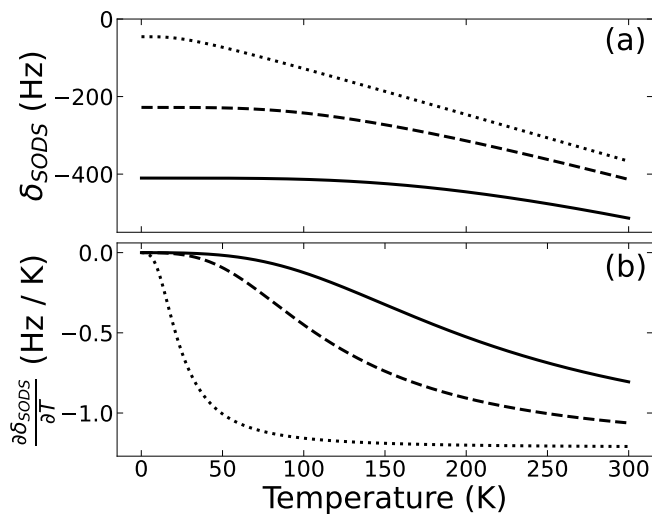


FIG. 5. The 2nd order Doppler shift (a) and its 1st temperature derivative (b) as a function of temperature. The dotted, dashed, and solid lines have a Debye temperature of 100, 500, and 900 K, respectively.

Electric Quadrupole Shift

A changing lattice volume will change the EFG experienced by the nucleus, thus changing the electric quadrupole splitting. While it is difficult to calculate the EFG as a function of temperature for an arbitrary crystal geometry, a common practice in Mößbauer literature spectroscopy is to fit the temperature dependence of the quadrupole splitting with a power law of the form: $\Delta E_Q(T) = \Delta E_Q(0)(1 - BT^{3/2})$, where $\Delta E_Q(0)$ is the quadrupole splitting at 0 K and B is an experimentally determined parameter. Common values of B found in the Mößbauer literature are around $10^{-5} K^{-3/2}$ [59–62]. Figs. 6a and 6b show the electric quadrupole splitting and its 1st temperature derivative as a function of temperature for various common values of B . Similar to the SODS, at low enough temperature, the temperature dependence of the electric quadrupole splitting becomes negligible.

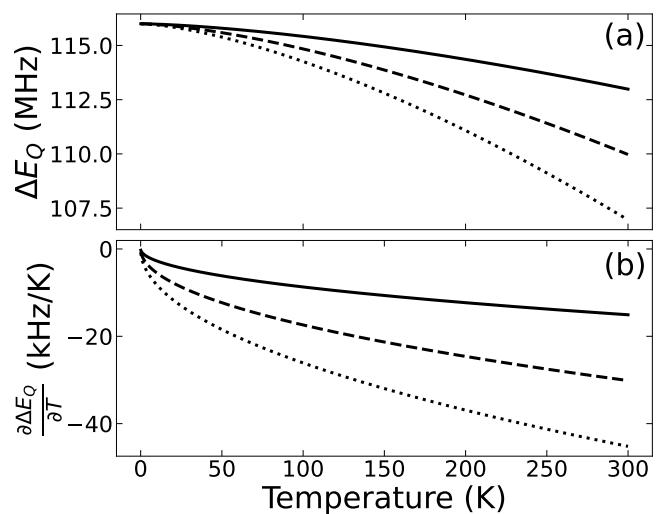


FIG. 6. The electric quadrupole splitting (a) and its 1st temperature derivative (b) as a function of temperature as described by an empirically determined power law. The dotted, dashed, and solid lines have a B of 5×10^{-6} , 10×10^{-6} , and $15 \times 10^{-6} K^{-3/2}$, respectively.